

Fig. 2 True fractional abundances maps of five endmembers for (top row) DC1 and (bottom row) DC2. From left to right: endmembers #1–#5

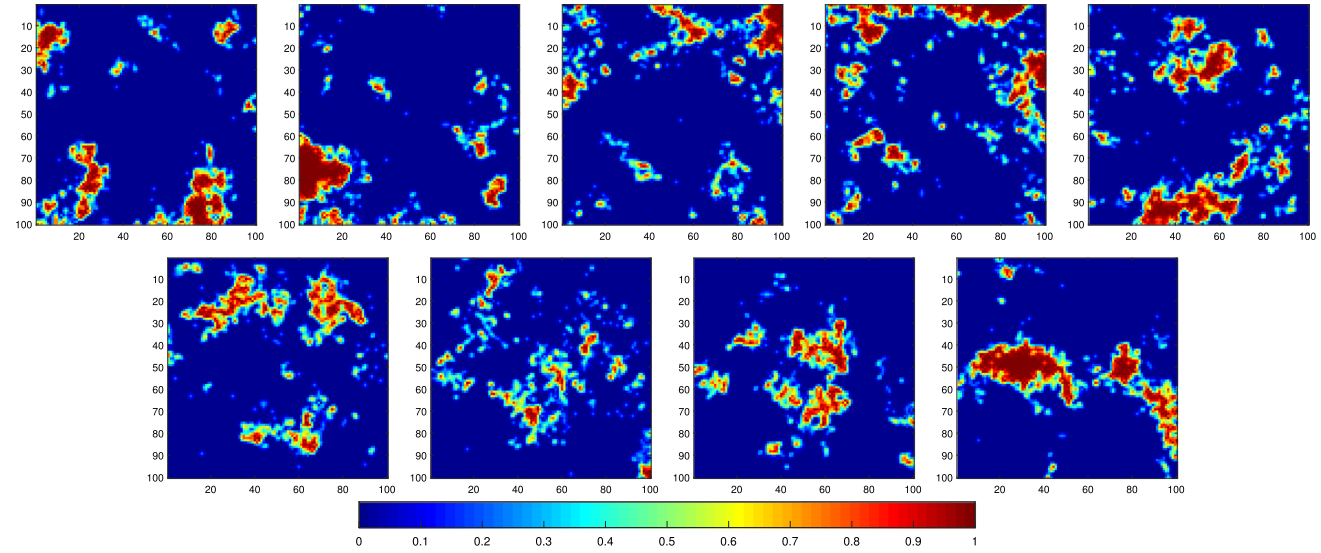


Fig. 3 True fractional abundances maps of nine endmembers in DC3. Top row: endmembers #1–#5. Bottom row: endmembers #6–#9

active endmembers have a larger degree of collaborativity and nonactive ones have a smaller, or ideally zero, degree of collaborativity. Figure 4 shows the degrees of collaborativity by SUNSAL-TV and SUNSAL-TV-MSD at 10th, 50th, 100th, and 200th iterations for DC1 with SNR = 40 dB. We see from Fig. 4 that as iteration goes, SUNSAL-TV detects most active endmembers with close degree of collaborativity to the true values but for nonactive endmembers, the degrees of collaborativity, which are supposed to be zero, are infected by perturbations. The proposed SUNSAL-TV-MSD algorithm provides more accurate degrees of collaborativity for both active and nonactive endmembers. In addition, we plot the number of active endmembers by SUNSAL-TV-MSD versus iteration for DC1 with SNR = 30 dB in Fig. 5a. It says

that MSD effectively reduces the active endmembers as iteration goes. Finally, Fig. 5b shows the convergence behavior of SUNSAL-TV with and without MSD. It shows again that MSD effectively improves the unmixing accuracy as iteration goes.

Moreover, Table 1 lists the SRE, RMSE, and the elapsed CPU time in seconds (denoted as Time (s)) by all compared algorithms. The best results for each quality index are highlighted in bold. It shows that most MSD-based algorithms provide higher SRE and lower RMSE values compared with the original ones, except for one case (JSBBLRU-MSD for DC2). Clearly, applying MSD reduces the computational time for all cases. Particularly, compared with SUNSAL-TV, SUNSAL-TV-MSD provides better SRE and RMSE val-

Fig. 4 Comparison of degrees of collaborativity of the ground truth and the estimations by SUnSAL-TV and SUnSAL-TV-MSD for DC1 with SNR = 40 dB

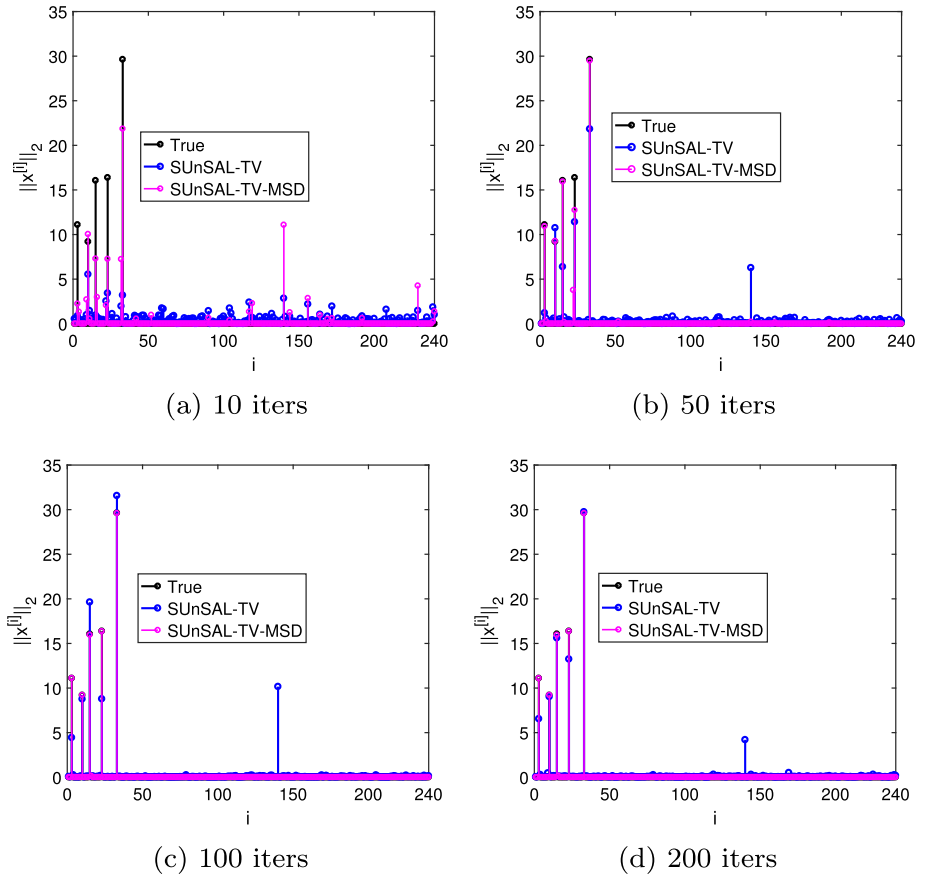
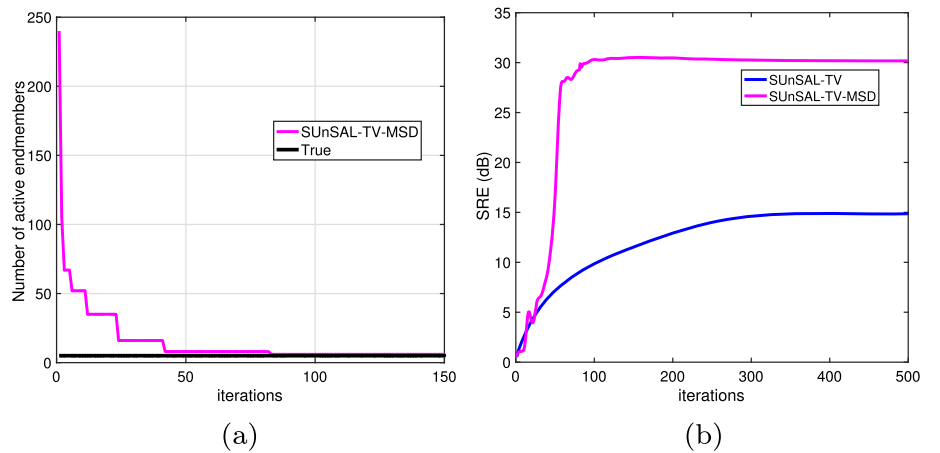


Fig. 5 Results of SUnSAL-TV-MSD against iteration for DC1 with SNR = 30 dB. **a** Number of active endmembers in SUnSAL-TV-MSD. **b** Convergence behavior comparison between SUnSAL-TV and SUnSAL-TV-MSD



ues with less computation time. It can be expected since SUnSAL-TV applies difference operators on all abundance maps corresponding to both active and nonactive endmembers, while SUnSAL-TV-MSD only applies on abundance maps corresponding to detected active endmembers.

Furthermore, Figs. 6, 7 and 8 show estimated abundance maps by SUnSAL-TV and SUnSAL-TV-MSD for simulated data cubes. Note that we select endmembers #5 and #6 in DC3 in Fig. 8 for space consideration and other endmembers show a similar conclusion. From Figs. 6, 7 and 8, we observe that

SUnSAL-TV-MSD provides more accurate abundance maps for SNR = 30 dB. In addition, Fig. 8 shows that the two algorithms provide overall similar estimations for SNR = 40 dB. Figure 9 shows estimated abundance maps by other MSD-based unmixing algorithms, compared with original ones. The improvement by SUnSAL-MSD and CLSUnSAL-MSD is clear, particularly for higher noise levels. We also note that estimated abundance maps by ADSpLRU-MSD and JSpBLRU-MSD are similar with those by original ones, which is consistent with the observations from Table 1. How-

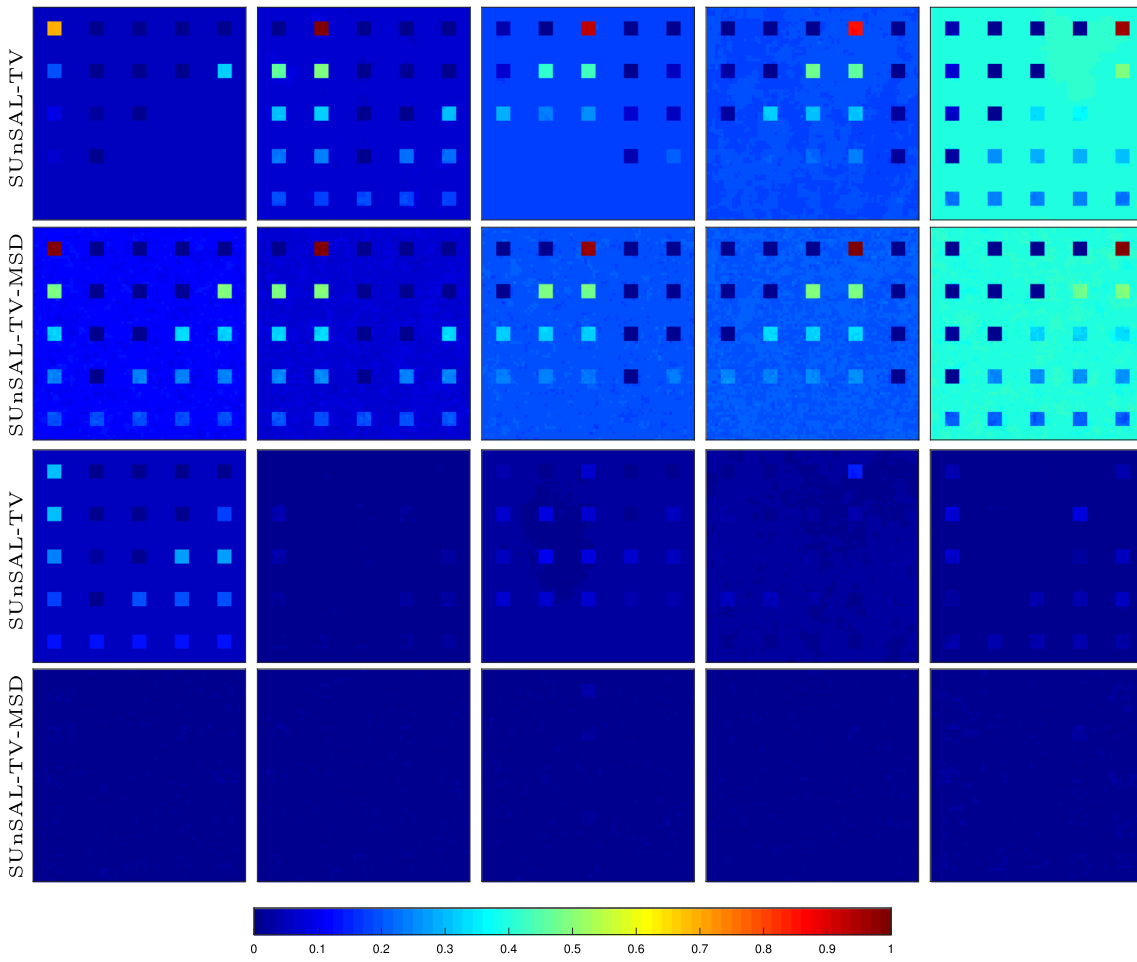


Fig. 6 Abundance maps obtained by SUnSAL-TV and SUnSAL-TV-MSD for (from left to right) endmembers #1–#5 in DC1 with SNR = 30 dB. The first two rows: estimated abundance maps. The last two rows: difference maps between the ground truth and the estimations

becomes more apparent when the SNR is slow. Table 2 lists the values of ϵ , which are chosen by trial and error, in different MSD-based algorithms for DC1–DC3. We note from this table that the selection of ϵ for each MSD-based algorithm is relatively stable for different date cubes and noise levels. We also note that the value of ϵ depends on the algorithm considered and so it should be carefully tuned in practice.

With different values of μ , Fig. 12 shows the changes of SRE values and number of active endmembers as iteration goes. We note that for each noise level, only values of μ vary and the same optimal values of λ and λ_{TV} are used. Figure 12 shows that the penalty parameter μ impacts the convergence speed and unmixing performance, similarly as in the standard ADMM iterates. Also when the value of μ becomes too large or too small, the convergence speed is slow, see the plots for $\mu = 0.001$ and 1 in Fig. 12. Moreover, we see from Fig. 12 that at first 50 iterations, the number of active endmembers decreases quite fast and the SRE values keep rising for all cases. As iteration goes, the number of active endmembers becomes stable or decreases very slowly and SRE values

clearly show sudden jumps as the number of active endmembers decreases. Commonly, the best SRE values are attained with an accurate number of active endmembers; see Fig. 12d, e and i. That is to say, an accurate estimation of number of active endmembers plays an important role in improving the unmixing performance. In addition, the smaller SNR value, the higher optimal value of μ .

Comparisons between MSD and a Pre-select Library. It has been shown that applying methods such as SUnSAL-TV with the original endmember matrix leads to slow convergence and high computational costs. Here we compare SUnSAL-TV with different methods employed on the initial spectral library, including the original SUnSAL-TV algorithm (with the initial spectral libraries used in DC1–DC3), SUnSAL-TV with the MSD method, i.e., SUnSAL-TV-MSD, and SUnSAL-TV with a pre-select spectral library. To pre-select the spectral library, we first apply a pre-processing step on the estimated abundance matrix, denoted as \mathbf{X}_0 , by the SUnSAL algorithm, which is very fast. Then we calculate the degree of collaborativity of \mathbf{X}_0 , i.e., $\phi(\mathbf{X}_0) =$

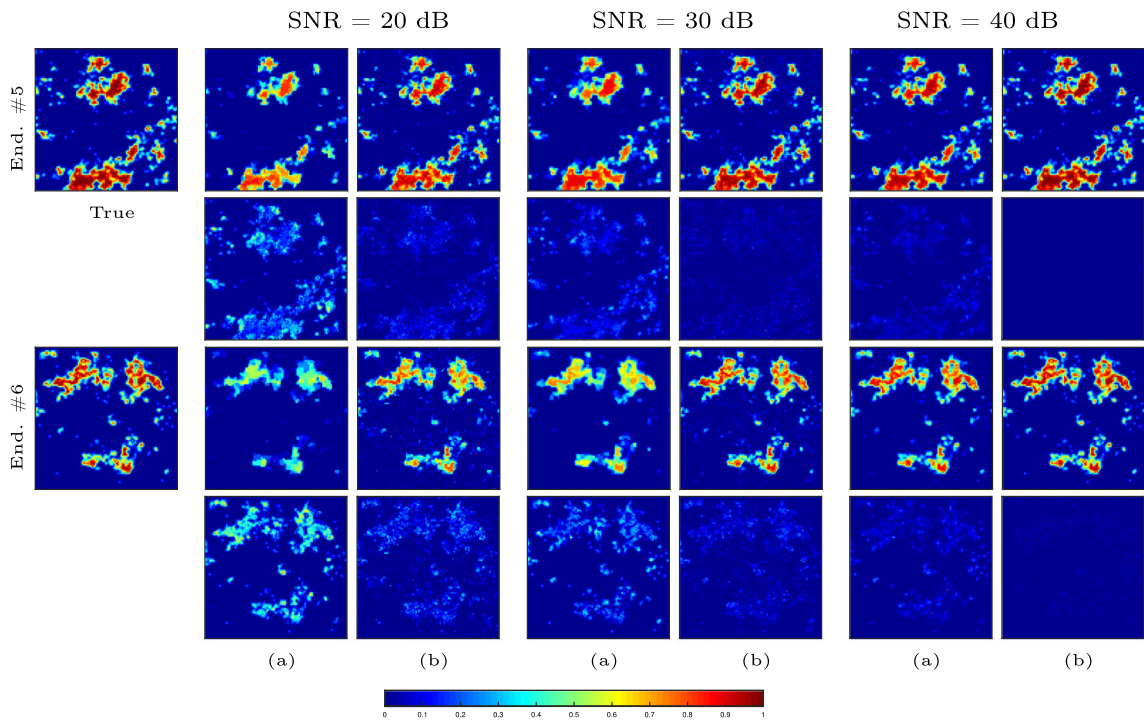


Fig. 8 Abundance maps obtained by **a** SUnSAL-TV and **b** SUnSAL-TV-MSD for endmembers #5 and #6 in DC3 with different SNR values. The first and third rows show the estimated abundance maps, and the second and last rows show the corresponding difference

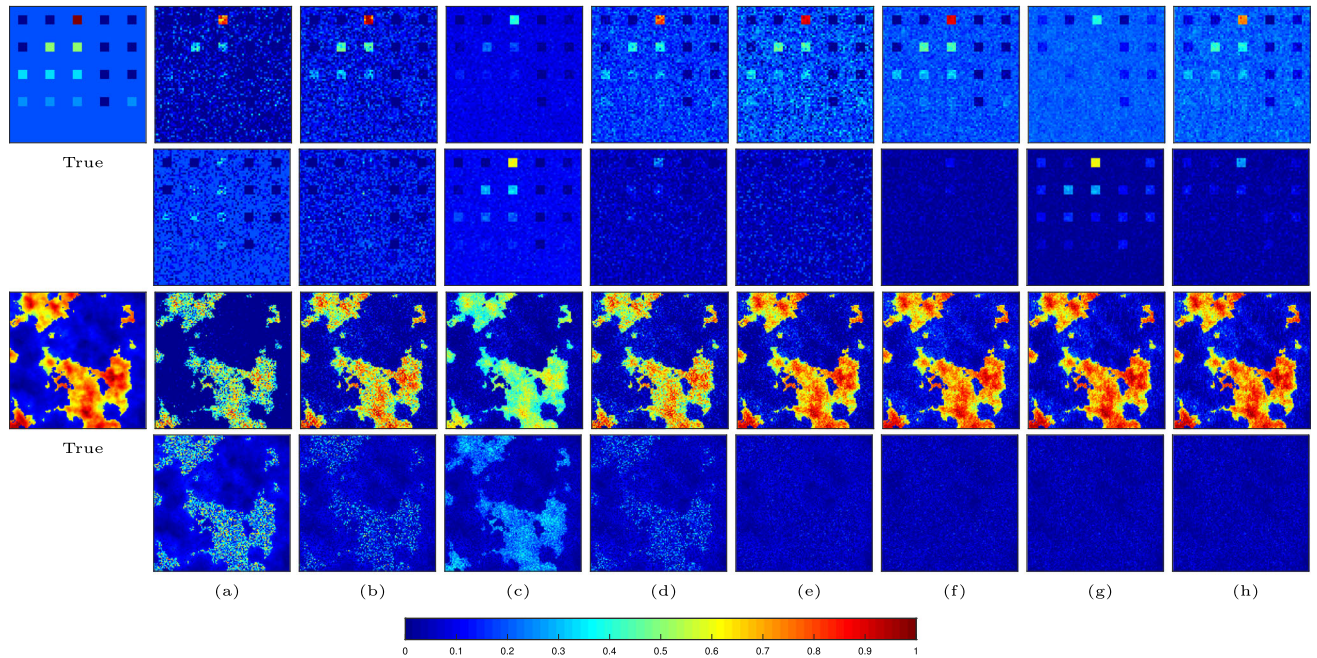
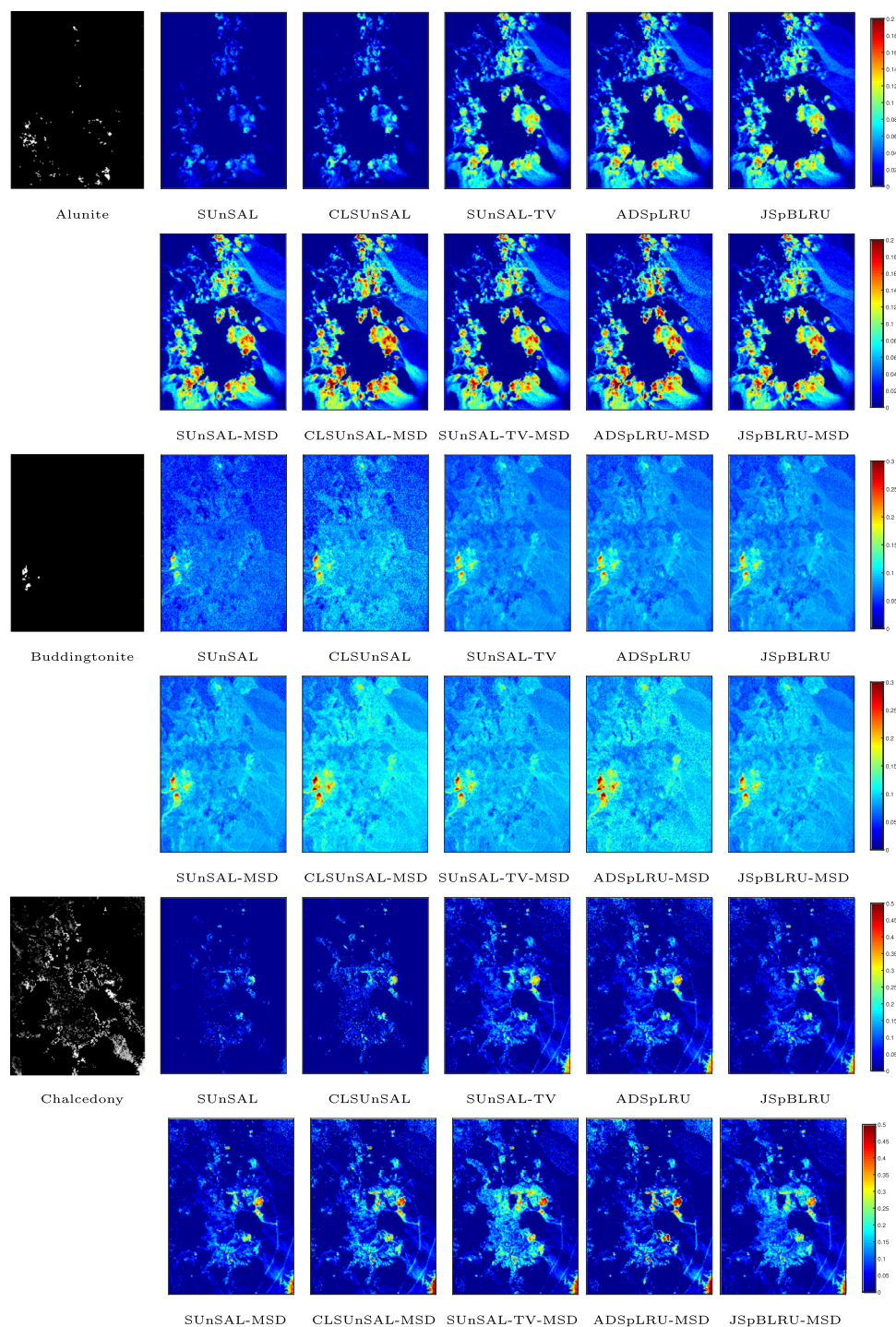


Fig. 9 Abundance maps obtained by different unmixing algorithms for (the first two rows) endmember #3 in DC1 and (the last two rows) endmember #5 in DC2 with SNR = 20 dB. The first and third rows show the estimated abundance maps and the second and last rows show

the difference maps. **a** SUnSAL. **b** SUnSAL-MSD. **c** CLSUnSAL. **d** CLSUnSAL-MSD. **e** ADSpLRU. **f** ADSpLRU-MSD. **g** JSpBLRU. **h** JSpBLRU-MSD

Fig. 13 References and estimated abundance maps by different unmixing algorithms for three minerals in the AVIRIS cuprite data cube





Jie Huang received the Ph.D. degree in applied mathematics from the University of Electronic Science and Technology of China (UESTC), Chengdu, China, in 2013. Currently, she is a Professor with the School of Mathematical Sciences, UESTC. Her research interests include remote sensing and image processing.



Liang-Jian Deng (Senior Member, IEEE) received the B.S. and Ph.D. degrees in applied mathematics from the School of Mathematical Sciences, University of Electronic Science and Technology of China (UESTC), Chengdu, China, in 2010 and 2016, respectively. From 2013 to 2014, he was a joint-training Ph.D. student with Case Western Reserve University, Cleveland, OH, USA. In 2017, he was a Post-Doctoral Researcher with Hong Kong Baptist University (HKBU), Hong Kong. He is currently a Research Fellow with the School of Mathematical Sciences, UESTC. In addition, he also stayed at the Isaac Newton Institute for Mathematical Sciences, University of Cambridge, Cambridge, U.K., and HKBU, for short visits. His research interests include machine learning, variational image processing, image fusion, etc. For more information, see <https://liangjiandeng.github.io/>.



Shuang Liang received the M.S. degree from the University of Electronic Science and Technology of China (UESTC), Chengdu, China, in 2022. Her research interests include remote sensing and image processing.